Low-Profile Epsilon-Near-Zero (ENZ) Cavity Antenna Array for Wide-Angle Beam Scanning

Zhenyu Liu, *Graduate Student Member, IEEE*, Yongjian Zhang, Wangyu Sun, and Yue Li, *Senior Member, IEEE*

***Abstract*—In this letter, a low-profile epsilon-near-zero (ENZ) cavity antenna array is proposed to achieve wide-angle beam scanning. The proposed array utilizes four slot-fed cavity antenna elements that operate with the ENZ mode, in which the electric field presents a unique sign-function-like distribution. By properly designing the width of the ENZ cavity, a wide 3 dB beamwidth is achieved in a low profile to increase the beam scanning angle of the array configuration. Furthermore, the narrow width of the antenna element also facilitates a decreased spacing between array elements, enabling the use of the appropriate spacing to increase the scanning angle. Different from the conventional wide-angle beam-scanning arrays with high profile, the proposed ENZ cavity antenna array achieves a remarkable beam scanning angle of $\pm 72^\circ$ ($\pm 73^\circ$ in the measurement) while maintaining a low profile of only 0.03 λ_0, exhibiting the potential applications in low-profile phased array systems.**

***Index Terms*—Antenna array radiation pattern, antenna arrays, epsilon near zero, low profile, wide-angle beam scanning.**

I. Introduction

With rapid progress in mobile communication technologies, wide-angle beam scanning antennas [1], [2], [3], [4] play an important role in wireless systems. By providing broader beam coverage in both azimuthal and elevated planes, the wide-angle beam scanning antennas enable wide-range dynamic adjustment of beam direction in response to changing propagation conditions. This adaptability results in improved signal reception, reduced interference, and increased system capacity, making wide-angle beam scanning antennas an ideal choice for serving multiple users simultaneously. Moreover, the ability to scan a wide beam angle also benefits positioning applications and radar systems. Additionally, the wide-angle beam scanning antennas simplify the hardware complexity, reduce power consumption, and offer robustness to the multipath fading. Nevertheless, conventional wide-angle beam scanning antenna arrays usually rely on high-profile structures [5], [6], [7], [8], [9], which occupy large volumes. Designing the elements with wide beamwidth is a key issue in realizing the phased array for wide-angle beam scanning.

Various methods have been developed for this purpose [10], [11], [12], [13], [14], and can be categorized into three approaches. The first approach applies a high profile for dielectric resonator antennas (DRA) or magnetoelectric dipole antennas. As an example, researchers in [15] apply a DRA featuring an incised groove and a metal wall with a comb-like pattern to augment the beamwidths in the E- and H-planes. Correspondingly, a dual-polarized magnetoelectric dipole antenna has been designed with the intention of enhancing the gain at lower elevation angles, thereby effectively broadening the beamwidth [16]. Additionally, the use of a thick substrate enhances the antenna bandwidth. The second one to achieve wide beamwidth adopts the parasitic units close to the primary radiator [17], [18], [19], [20], [21]. These structures could efficiently reimburse radiation and enhance the beamwidth, at the expense of larger volumes. The third one involves reshaping the antenna's ground plane, i.e., altering its dimensions [22], [23], [24] or bringing in a three-dimensional ground plane beneath the patch antenna [25], [22]. This approach broadens the beamwidth by involving ground edge currents in the radiation. However, it may introduce a strong back lobe and a front-to-back ratio not exceeding 10 dB. Based on the discussion of the existing methods, it is still a challenge to achieve wide beam coverage within a low antenna profile.

In this letter, we present a feasible approach to achieve wide-angle beam scanning with a low profile using an epsilon-near-zero (ENZ) cavity antenna array. For the element design, the wide beamwidth is achieved by utilizing the properly designed ENZ cavity while maintaining an overall profile of the antenna structure below 0.03 λ_0. Furthermore, by assembling four ENZ cavity antenna units as the phased array configuration, wide-angle beam scanning capability is achieved within the whole operating band.

II. Antenna Design

Fig. 1 illustrates the geometry of the proposed antenna, which is composed of two dielectric layers and three metal layers. The antenna can be divided into two parts. The first part is the slot-fed substrate integrated waveguide (SIW) antenna, consisting of a top ENZ metalized patch (Metal Layer 1), an SIW cavity with loaded shorting vias (Substrate Layer 1), and a feeding slot (Metal Layer 2). The second part is the back-cavity structure excited by microstrip to coplanar waveguide (CPW) transition, consisting of an SIW cavity with shorting vias around the

Manuscript received 17 January 2024; revised 1 March 2024; accepted 23 March 2024. Date of publication 28 March 2024; date of current version 9 July 2024. This work was supported in part by the National Natural Science Foundation of China (NSFC) under Grant U22B2016; in part by the National Key Research and Development Program of China under Grant 2021YFA0716601; and in part by Shenzhen Science and Technology Program under Grant JSGG20210802153800002. *(Corresponding author: Yue Li.)*

Zhenyu Liu, Yongjian Zhang, and Yue Li are with the Department of Electronic Engineering, Beijing National Research Center for Information Science and Technology, Tsinghua University, Beijing 100084, China (e-mail: lyee@tsinghua.edu.cn).

Wangyu Sun is with the Aerospace Information Research Institute, Chinese Academy of Sciences, Beijing 100190, China.

Digital Object Identifier 10.1109/LAWP.2024.3382290

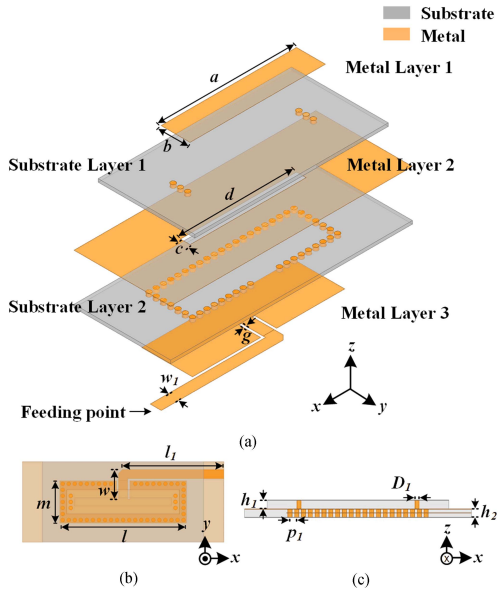

Fig. 1. Configuration of the proposed antenna element: (a) perspective view; (b) top view; and (c) cross-sectional view.

TABLE I
DETAILED DIMENSIONS

Parameter	Value (mm/λ_0)	Parameter	Value (mm/λ_0)	Parameter	Value (mm/λ_0)
a	87.3 mm (0.71 λ_0)	b	18.7 mm (0.15 λ_0)	c	6.2 mm (0.05 λ_0)
d	74.9 mm (0.61 λ_0)	l_1	78.0 mm (0.63 λ_0)	w	22.8 (0.19 λ_0)
m	32.7 mm (0.27 λ_0)	l	98.3 mm (0.80 λ_0)	D_1	3.1 mm (0.03 λ_0)
h_1	2 mm (0.016 λ_0)	h_2	2 mm (0.016 λ_0)	d_1	42.4 mm (0.35 λ_0)
p_1	4.7 mm (0.04 λ_0)	g_1	1.6 mm (0.013 λ_0)	w_1	7.1 mm (0.06 λ_0)

λ_0 is the operating wavelength of the antenna in the free space @2.44 GHz

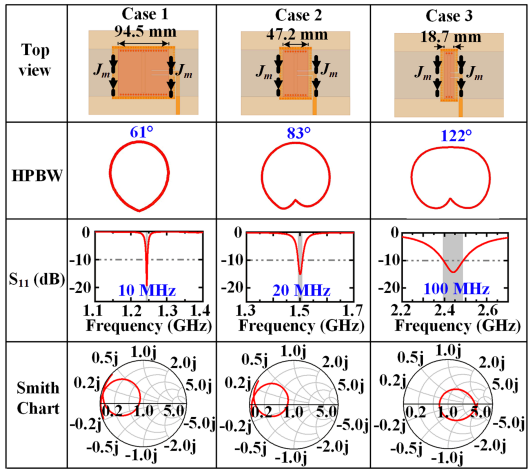

Fig. 2. Comparison of HPBW of H-plane radiation pattern and simulated S_{11} and Smith chart of the proposed antenna with different values of b.

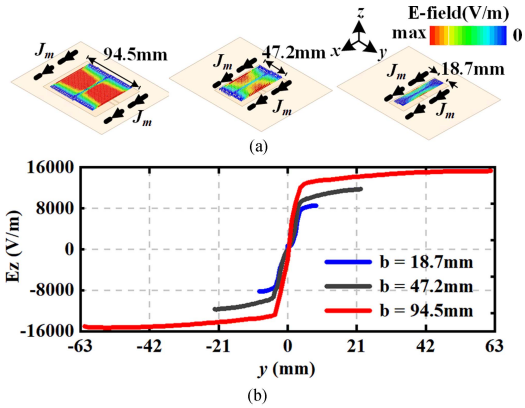

Fig. 3. (a) Simulated electric field distribution of the antenna with different b; and (b) normalized electric field along z-direction on the center plane at different locations along the y-axis with variation to b.

perimeter (Substrate Layer 2) and a CPW feeding structure (Metal Layer 3). All shorting vias in the structure have a diameter of d_1, and the spacing between adjacent shorting vias is p_1. A microstrip line of length l_1 extends from the side of the bottom layers. Subsequently, it bends 90° at the center and excites the back cavity from the bottom through a coplanar waveguide (CPW) with a length of w_1 and gaps of g_1. At the top of the back cavity, a narrow slot is created, ultimately exciting the ENZ metalized patch on the top layer. The ENZ metalized patch is fabricated on a 2 mm thick F4B substrate with a relative permittivity of 2.65 and loss tangent of 0.002. Table I presents the parameter values.

To identify the optimal structure of the element radiation pattern and explain the method for achieving wide beamwidth of the proposed antenna, Fig. 2 presents a comparison of the half-power beamwidth (HPBW) of the H-plane radiation pattern and the simulated S_{11} and Smith chart of the proposed antenna with different widths $\boldsymbol{b}$ of the ENZ antenna. As the spacing between magnetic currents gradually decreases from 94.5 mm to 18.7 mm, the HPBW of the antenna increases from 61° to 122°. Through the examination of the electric field distribution of the proposed antenna and the Huygens equivalence principle, it can be inferred that the radiation pattern of the antenna can be approximately represented as the array pattern generated by the two parallel magnetic currents in the same phase at the antenna radiation aperture. As we know, the radiation pattern of the array is equal to the product of the element factor and array factor. According to [10], it is known that a smaller magnetic current spacing results in a wider beamwidth of the antenna due to the wide beamwidth radiation pattern of the array factor formed by the two magnetic currents. In addition, during this process, the S_{11} on the Smith chart is rotated clockwise (from left size to right size) due to the stronger capacitance loading effect of the back cavity.

Fig. 3 shows three electric field distributions with different widths with the $\boldsymbol{Ez}$ component inside the cavity. First, it can be observed that under the three cases, the electric field distribution on both sides of the slot presents the same magnitude and phase, with only a phase reversal at the slot position, exhibiting an electric field distribution reminiscent of a signum function inside the cavity. To establish a distinction from the ENZ modes employed in earlier instances [26], [27], [28], [29], [30], [31], we classify the discussed mode as the AP-ENZ (antiphase-ENZ) mode due to the out-of-phase character of the electric field on two sides of the slot. The interpretation of the specific AP-ENZ mode is as follows. ENZ, which stands for epsilon near zero metamaterial, refers to materials with dielectric constants close to zero. We here physically realize ENZ metamaterials based on the structural dispersions of waveguides. The wave propagation

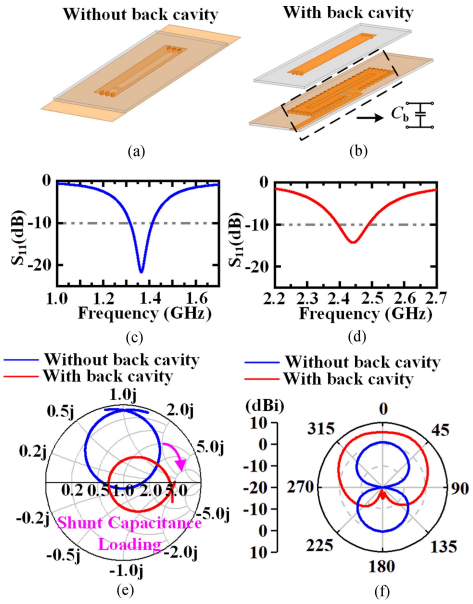

Fig. 4. Schematic diagram of with and without loading the back cavity on the ENZ antenna: Antenna configuration (a) without and (b) with the back cavity. Simulated S_{11} (c) without and (d) with the back cavity. (e) Smith chart and (f) H-plane radiation pattern of the ENZ antenna with and without a back cavity.

along the middle plane inside the waveguide can be made an analogy to plane-wave propagation in an equivalent homogeneous material with an effective permittivity $\varepsilon_{eff} = \varepsilon_r - 4c^2f^2/W^2$ [26]. Here, $\boldsymbol{c}$ represents the speed of light; $\boldsymbol{W}$ stands for the width of the waveguide, and ε_r signifies the relative permittivity of the internal medium. Based on this relation, we can conclude that at the cutoff frequency f_{c10} of the TE_{10} mode, the effective permittivity becomes near zero. This allows the waveguide to exhibit propagation characteristics identical to those of an ENZ medium at f_{c10}, including infinite wavelength and a near-zero propagation constants β.

The reason ENZ structures can achieve wide beamwidth and wide-angle beam scanning of the antenna is that ENZ is a structure with a uniformly distributed electric field. This allows us to infinitely reduce the dimensions of the ENZ structure in the dimension of width, as shown in Fig. 3, while maintaining the existence of the ENZ mode. As shown in Fig. 2, when we reduce the width dimension of the ENZ structure, the narrowing of the magnetic current distances results in wide beamwidth characteristics for the antenna element and thus can also achieve wide-angle beam scanning when forming the array. Besides, in the z-direction (height or profile direction), the electric field is also the zero-order modes, meaning the electric field is approximately uniform. Consequently, we can reduce the profile height without affecting the antenna's fundamental mode and radiation characteristics. Thus, we can utilize the low-profile structure of the proposed antenna.

Fig. 4 discusses the influence of the back cavity on the impedance and radiation of the ENZ antenna. First, we examine the impedance characteristics. As indicated in reference [26], for the frequency calculation of the ENZ antenna without a back cavity, the resonant frequency of the antenna is calculated to be around 1.2 GHz, which is close to the simulated resonant frequency of the antenna. Considering the ENZ antenna as the main radiator, the back cavity can be treated as a loading element in the equivalent circuit. Comparing the Smith charts in Fig. 4(e), it can be observed that the impedance curve of the ENZ antenna

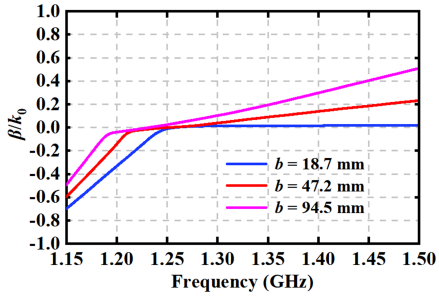

Fig. 5. Dispersion diagram for the top-layer patch under three cases.

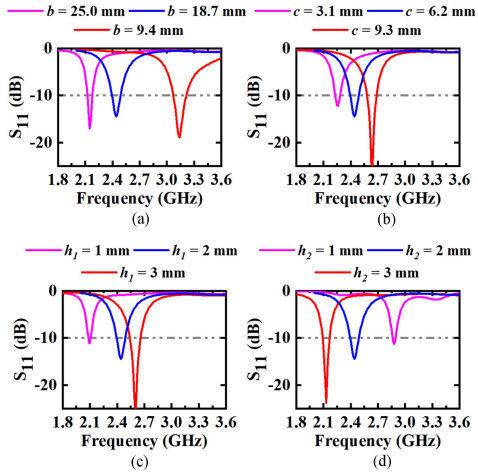

Fig. 6. Key parameter discussion including (a) parameter b, (b) parameter c, (c) parameter h1, and (d) parameter h2 of the proposed antenna element.

rotates clockwise and moves downward along the admittance circle after loading the back cavity. This indicates that the effect of the back cavity on the ENZ antenna can be approximated as that of a parallel capacitor, leading to an increase in the antenna's resonant frequency from 1.36 to 2.44 GHz. Besides, a back cavity can also enhance the front-to-back ratio. The dispersion diagram for the top layer patch under three cases is shown in Fig. 5. From the dispersion diagram, it can be observed that all the three propagations constants β undergoes a transition from negative to positive values. The region around β near zero is equivalent to the ENZ mode formed by the cutoff mode of the waveguide TE_{10} mode. The key parameter discussion of the proposed antenna element is shown in Fig. 6.

III. Result

On the basis of the previously optimized antenna element, a 4-element array is formed with a spacing of $\boldsymbol{d_1}$ for wide-angle beam scanning applications. A prototype of an array is also constructed and examined to confirm the design's validity. Corresponding to the depiction in Fig. 7, an SMA connector is soldered between the bottom metal ground and the middle metal ground to feed the antenna. As presented in Fig. 8, the measured S_{11} aligns favorably with the simulated result. Within the frequency range of 2.39 to 2.49 GHz, both the measured and simulated S_{11} exhibit values below -10 dB. The isolation between different ports of the antenna is below -15 dB, indicating low coupling between different ports of the antenna. In the operating band, the total efficiencies attained from simulation and measurement surpass 82% and 77%, respectively. Fig. 9 shows the simulated and measured results of the beam scanning

TABLE II
COMPARISON AMONG THE PROPOSED DESIGN AND OTHER RELATED ANTENNAS

Reference	Antenna Type	Element Number	Array gain (dBi)	Efficiency	Element Size (λ_0^2)	Profile (λ_0)	3-dB Beam Scanning Angle
[32]	Patch	9	12.5	/	0.35×0.43	0.24	–70°~70°
[33]	Cross-dipole	8	14.4	87%	0.50×0.50	0.11	–65°~65°
[34]	Patch	9	16.2	/	0.31×0.40	0.09	–60°~60°
[35]	Slot	9	14.6	/	0.71×1.13	0.05	–50°~50°
[36]	DRA	4	9.0	81%	0.32×0.22	0.09	–65°~65°
[37]	Dipole	8	13.0	50%	0.22×0.19	0.15	–60°~60°
Proposed	**ENZ**	**4**	**11.0**	**82%**	**0.34×0.80**	**0.03**	**–73°~73°**

The bold entities represents various performance metrics of proposed work (our work).

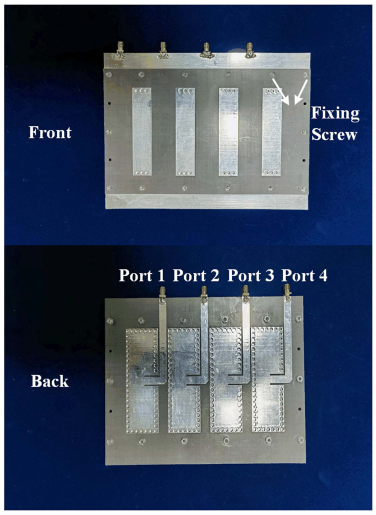

Fig. 7. Photograph of the fabricated prototype of the proposed antenna array.

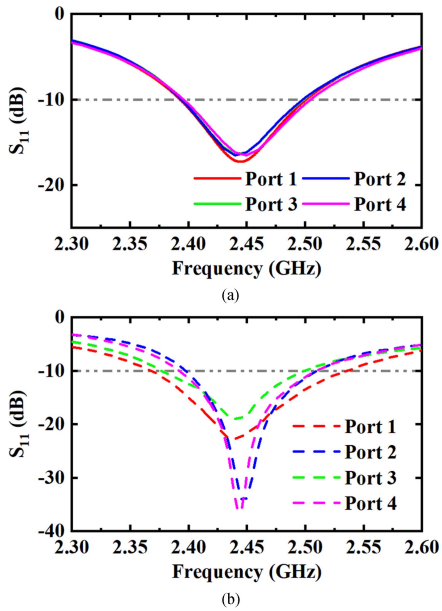

Fig. 8. (a) Simulated and (b) measured S_{11} of the proposed antenna array.

angles. It can be seen that the 3 dB beam scanning angles from the simulated result and the measured result are in close agreement, with values of ±72° and ±73°, respectively. To highlight the innovation and performance advantages of the proposed antenna array, Table II provides the performance comparisons, including antenna type, element size, profile, and 3 dB beam scanning

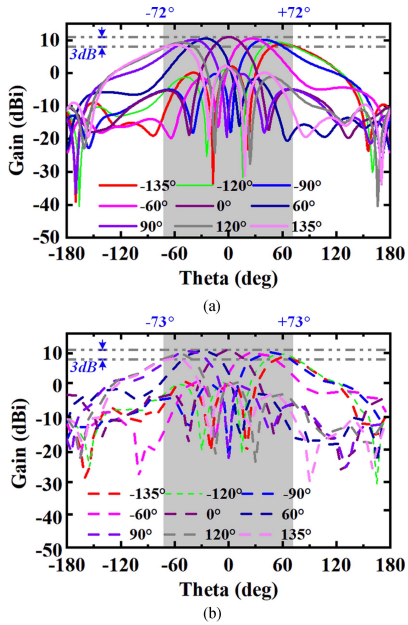

Fig. 9. Scanning performance at 2.44 GHz in the H-plane (yoz plane) of the proposed antenna array. (a) Simulated results. (b) Measured results.

angle. It can be observed that the microstrip antenna in [32] realizes a beam scanning angle of ±70° within a high profile close to 1/4 wavelength. The low-profile designs in [35] achieve narrow beam scanning angles of ±50°. Therefore, based on other references, there is a clear contradiction between the antenna profile and the beam scanning coverage angle. The proposed antenna, employing the ENZ mode, has shown simultaneous improvements in both profile and beam scanning angle compared to previous works, addressing the intrinsic contradiction between antenna profile and beam scanning angle.

IV. CONCLUSION

In this letter, we present a wide-angle beam scanning antenna array based on four identical low-profile wide-beamwidth ENZ elements. By utilizing the slot-excited anti-phase ENZ mode with the properly reduced width, the proposed antenna element achieves wide beamwidth characteristics. Furthermore, based on the designed element, a 4-element array is constructed, simultaneously providing a low profile of 0.03 λ_0 and a wide beam scanning angle of ±72°. The measured results show that the antenna array achieves a ±73° beam scanning angle. Therefore, the proposed approach holds the potential to pave a promising path for profile-limited and conformal phased array designs in confined spatial environments.

REFERENCES

[1] H. Wu et al., "A low-profile wideband dual-polarized antenna based on an improved HIS and its broad-angle beam-scanning array," *IEEE Antennas Wireless Propag. Lett.*, vol. 19, no. 3, pp. 383–387, Mar. 2020.

[2] Y.-Q. Wen, S. Gao, B.-Z. Wang, and Q. Luo, "Dual-polarized and wide-angle scanning microstrip phased array," *IEEE Trans. Antennas Propag.*, vol. 66, no. 7, pp. 3775–3780, Jul. 2018.

[3] P. Zhang, S.-W. Qu, and S. Yang, "Dual-polarized planar phased array antenna with cavity-backed elements," *IEEE Antennas Wireless Propag. Lett.*, vol. 18, no. 9, pp. 1736–1740, Sep. 2019.

[4] T. Chaloun, V. Ziegler, and W. Menzel, "Design of a dual-polarized stacked patch antenna for wide-angle scanning reflectarrays," *IEEE Trans. Antennas Propag.*, vol. 64, no. 8, pp. 3380–3390, Aug. 2016.

[5] M. Boyuan, J. Pan, S. Huang, D. Yang, and Y. Guo, "Wide-beam dielectric resonator antennas based on the fusion of higher-order modes," *IEEE Trans. Antennas Propag.*, vol. 69, no. 12, pp. 8866–8871, Dec. 2021.

[6] S. H. H. Mashhadi, Y. Jiao, and J. Chen, "Broadbeam cylindrical dielectric resonator antenna," *IEEE Access*, vol. 7, pp. 112653–112661, 2019.

[7] Z. N. Chen and M. Y. W. Chia, "Broad-band suspended probe-fed plate antenna with low cross-polarization levels," *IEEE Trans. Antennas Propag.*, vol. 51, no. 2, pp. 345–346, Feb. 2003.

[8] J. Row and Y. Chen, "Wideband planar array with broad beamwidth and low cross-polarization," *IEEE Trans. Antennas Propag.*, vol. 63, no. 9, pp. 4161–4165, Sep. 2015.

[9] K. B. Ng, C. H. Chan, and K.-M. Luk, "Low-cost vertical patch antenna with wide axial-ratio beamwidth for handheld satellite communications terminals," *IEEE Trans. Antennas Propag.*, vol. 63, no. 4, pp. 1417–1424, Apr. 2015.

[10] Z. Liu, Y. He, and Y. Li, "Beamwidth enhancement of microstrip antennas using capacitive via-fence loading," *IEEE Open J. Antennas Propag.*, vol. 4, pp. 151–158, 2023.

[11] Y. Zhang, Z. Xue, and W. Hong, "Planar substrate-integrated endfire antenna with wide beamwidth for Q-Band applications," *IEEE Antennas Wireless Propag. Lett.*, vol. 16, pp. 1990–1993, 2017.

[12] Y. Zhang and Y. Li, "Wideband microstrip antenna in small volume without using fundamental mode," *Electromagn. Sci.*, vol. 1, no. 2, Jun. 2023, Art. no. 0020073.

[13] Z. Liu, Y. Zhang, Y. He, and Y. Li, "A compact-size and high-efficiency cage antenna for 2.4-Ghz wlan access points," *IEEE Trans. Antennas Propag.*, vol. 70, no. 12, pp. 12317–12321, Dec. 2022.

[14] Y. Zhang, Y. Li, W. Zhang, Z. Zhang, and Z. Feng, "Omnidirectional antenna diversity system for high-speed onboard communications," *Engineering*, vol. 11, no. 4, pp. 72–79, 2022.

[15] R.-Y. Li, Y.-C. Jiao, Y.-X. Zhang, L. Zhang, and H.-Y. Wang, "A DRA with engraved groove and comb-like metal wall for beamwidth enhancement in both E- and H-Planes," *IEEE Antennas Wireless Propag. Lett.*, vol. 20, no. 4, pp. 543–547, Apr. 2021.

[16] J. Yin and L. Zhang, "Design of a dual-polarized magnetoelectric dipole antenna with gain improvement at low elevation angle for a base station," *IEEE Antennas Wireless Propag. Lett.*, vol. 19, no. 5, pp. 756–760, May 2020.

[17] G. Yang, J. Li, D. Wei, S. Zhou, and J. Yang, "Broadening the beamwidth of microstrip antenna by the induced vertical currents," *IET Microw., Antennas Propag.*, vol. 12, no. 2, pp. 190–194, Feb. 2018.

[18] Z. Chen, W. Toh, and X. Qing, "A microstrip patch antenna with broadened beamwidth," *Microw. Opt. Technol. Lett.*, vol. 50, no. 7, pp. 1885–1888, 2008.

[19] X. Chen, P.-Y. Qin, Y. Guo, and G. Fu, "Low-profile and wide beamwidth dual-polarized distributed microstrip antenna," *IEEE Access*, vol. 5, pp. 2272–2280, 2017.

[20] Z.-K. Pan, W.-X. Lin, and Q.-X. Chu, "Compact wide-beam circularly-polarized microstrip antenna with a parasitic ring for CNSS application," *IEEE Trans. Antennas Propag.*, vol. 62, no. 5, pp. 2847–2850, May 2014.

[21] G. Yang, J. Li, J. Yang, and S.-G. Zhou, "A wide beamwidth and wideband magnetoelectric dipole antenna," *IEEE Trans. Antennas Propag.*, vol. 66, no. 12, pp. 6724–6733, Dec. 2018.

[22] T. P. Wong and K. M. Luk, "A wide bandwidth and wide beamwidth CDMA/GSM base station antenna array with low backlobe radiation," *IEEE Trans. Veh. Technol.*, vol. 54, no. 3, pp. 903–909, May 2005.

[23] J. Mlynarczyk, "Wide-beam high-efficiency microstrip patch-based antenna for broadband wireless applications," *Microw. Opt. Technol. Lett.*, vol. 53, no. 2, pp. 286–288, Dec. 2010.

[24] C. Su, S. Huang, and C. Lee, "CP microstrip antenna with wide beamwidth for GPS band application," *Electron. Lett.*, vol. 43, no. 20, pp. 1062–1063, Sep. 2007.

[25] S. Noghanian and L. Shafai, "Control of microstrip antenna radiation characteristics by ground plane size and shape," *IEE Proc. Microw. Antennas Propag.*, vol. 145, no. 3, pp. 207–212, Jun. 1998.

[26] Z. Zhou and Y. Li, "Effective epsilon-near-zero (ENZ) antenna based on transverse cutoff mode," *IEEE Trans. Antennas Propag.*, vol. 67, no. 4, pp. 2289–2297, Apr. 2019.

[27] Z. Zhou et al., "Dispersion coding of ENZ media via multiple photonic dopants," *Light Sci. Appl.*, vol. 11, p. 207, 2022.

[28] Z. Hu, C. Chen, Z. Zhou, and Y. Li, "An epsilon-near-zero-inspired PDMS substrate antenna with deformation-insensitive operating frequency," *IEEE Antennas Wireless Propag.*, vol. 19, no. 9, pp. 1591–1595, Sep. 2020.

[29] Z. Liu, Z. Zhou, Y. Li, and Y. Li, "Integrated epsilon-near-zero antenna for omnidirectional radiation," *Appl. Phys. Lett.*, vol. 119, 2021, Art. no. 151904.

[30] H. Li et al., "Geometry-independent antenna based on epsilon-near-zero medium," *Nature Commun.*, vol. 13, 2022, Art. no. 3568.

[31] H. Li, Z. Zhou, Y. Zhao, and Y. Li, "Low-loss beam synthesizing network based on epsilon-near-zero (ENZ) medium for on-chip antenna array," *Chip*, vol. 2, 2023, Art. no. 100049.

[32] G. Yang, J. Li, S. G. Zhou, and Y. Qi, "A wide-angle E-Plane scanning linear array antenna with wide beam elements," *IEEE Antennas Wireless Propag. Lett.*, vol. 16, pp. 2923–2926, 2017.

[33] G. Yang and S. Zhang, "Dual-polarized wide-angle scanning phased array antenna for 5G communication systems," *IEEE Trans. Antennas Propag.*, vol. 70, no. 9, pp. 7427–7438, Sep. 2022.

[34] G. Yang, J. Li, R. Xu, Y. Ma, and Y. Qi, "Improving the performance of wide-angle scanning array antenna with a high-impedance periodic structure," *IEEE Antennas Wireless Propag. Lett.*, vol. 15, pp. 1819–1822, 2016.

[35] L. Gu, Y.-W. Zhao, Q.-M. Cai, Z.-P. Zhang, B.-H. Xu, and Z.-P. Nie, "Scanning enhanced low-profile broadband phased array with radiator-sharing approach and defected ground structures," *IEEE Trans. Antennas Propag.*, vol. 65, no. 11, pp. 5846–5854, Nov. 2017.

[36] Z. Wang, S. Zhao, and Y. Dong, "Metamaterial-based wide-beam dielectric resonator antenna for broadband wide-angle beam-scanning phased array applications," *IEEE Trans. Antennas Propag.*, vol. 70, no. 10, pp. 9061–9072, Oct. 2022.

[37] I. Syrytsin, S. Zhang, G. F. Pedersen, and A. S. Morris, "Compact quad-mode planar phased array with wideband for 5G mobile terminals," *IEEE Trans. Antennas Propag.*, vol. 66, no. 9, pp. 4648–4657, Sep. 2018.